

BIGPrior: Towards Decoupling Learned Prior Hallucination and Data Fidelity in Image Restoration

Majed El Helou, *Student Member, IEEE*, Sabine Süsstrunk, *Fellow, IEEE*.

Abstract—Image restoration, such as denoising, inpainting, colorization, etc. encompasses fundamental image processing tasks that have been addressed with different algorithms and deep learning methods. Classical image restoration algorithms leverage a variety of priors, either implicitly or explicitly. Their priors are hand-designed and their corresponding weights are heuristically assigned. Thus, deep learning methods often produce superior image restoration quality. Deep networks are, however, capable of strong and hardly-predictable hallucinations of the data to be restored. Networks jointly and implicitly learn to be faithful to the observed data while learning an image prior, and the separation of original data and hallucinated data downstream is then not possible. This limits their wide-spread adoption in image restoration applications. Furthermore, it is often the hallucinated part that is victim to degradation-model overfitting.

We present an approach with decoupled network-prior based hallucination and data fidelity terms. We refer to our framework as the Bayesian Integration of a Generative Prior (BIGPrior). Our BIGPrior method is rooted in a Bayesian restoration framework, and tightly connected to classical restoration methods. In fact, our approach can be viewed as a generalization of a large family of classical restoration algorithms. We leverage a recent network inversion method to extract image prior information from a generative network. We show on image colorization, inpainting, and denoising that our framework consistently improves the prior results through good integration of data fidelity. Our method, though partly reliant on the quality of the generative network inversion, is competitive with state-of-the-art supervised and task-specific restoration methods. It also provides an additional metric that sets forth the degree of prior reliance per pixel. Indeed, the per pixel contributions of the decoupled data fidelity and prior terms are readily available in our proposed framework.

Index Terms—Deep image restoration, data fidelity, network hallucination, learned prior.

I. INTRODUCTION

IMAGE restoration aims to recover original images from degraded observations. It is based on two fundamental aspects, namely, the relation to the observed data and the additional assumptions or image statistics that can be considered for the restoration. The relation to the observed data is what is referred to as *data fidelity*. The remaining information, brought in by the restoration method based on prior assumptions, is referred to as *prior hallucination*. It is termed as hallucination

since the added information is derived from a general model or assumption and might not faithfully match the sample image.

The data fidelity and prior terms emerge theoretically in the Maximum A Posteriori (MAP) formulation, but can also be implicitly induced by the restoration algorithms. For instance, non-local means [4] and BM3D [9] utilize the prior assumption that there exists different similar patches within an image. Diffusion [32] methods build on local smoothness assumptions. Data fidelity is typically enforced through the squared norm [24] that is equivalent to a MAP-based Gaussian noise model.

Classical image restoration algorithms often rely on optimizations over explicit priors. An advantage of explicitly-defined priors is the ability to easily control the relative relation between the weight of the data fidelity term and the weight (β) of the prior term. The general approach consists of an optimization

$$\arg \min_x \psi_d(f'(x), y) + \beta \cdot \psi_p(f''(x)), \quad (1)$$

where y is the observation, f' and f'' are various manipulation functions, ψ_d enforces the data fidelity while ψ_p enforces the prior information. The optimal point is the estimate of the original image x . By making the prior term explicit, it is possible to have control over its contribution and thus often better intuition and understanding of the reliability of the final restoration result. We note, however, two shortcomings of these methods that we expand upon in what follows, (1) β is not adapted based on the confidence in the fitness of the prior, and (2) the priors are hand-designed heuristics.

(1) The parameter β should be inversely related to the quality of the observed degraded signal, but it should also be directly related to how well the assumed prior corresponds to the input image distribution or statistics. Although some methods, discussed in related work, adjust their priors to the input data, they do not control β based on the confidence in the fitness of the prior to the current sample. (2) Recent methods with implicit data-learned priors, notably relying on deep CNNs, outperform the classical methods with hand-designed priors on various image restoration tasks. This is due to the rich prior learned by discriminative networks, or generative networks with adversarial training that can even learn image distributions to synthesize new realistic photos [21], [22], [23]. It is worth noting, however, that domain-specific prior information can still be explicitly enforced to improve the performance of the networks [15], [39].

Both authors are with the School of Computer and Communication Sciences, EPFL, Lausanne, Switzerland.

Contact author's email address: majed.elhelou@epfl.ch

Our code and models are made publicly available at:

<https://github.com/majedelhelou/BIGPrior>

One shortcoming of the deep learning methods is, however, the loss of interpretability and control between data fidelity and prior-based hallucination. Given an image restored by a network, it is not possible to know how faithful it is to the observed signal, versus how much prior-based hallucination was integrated in the image. And these hallucinations are not always reliable and can be prone to overfitting [16]. Hence the importance of having a grasp over the prior hallucination taking place in the restoration process.

To obtain decoupled prior-based hallucination and data fidelity terms, we propose a novel framework, which we call the **Bayesian Integration of a Generative Prior** (BIGPrior framework). We replace the implicit data prior learned in feed-forward restoration networks with an explicit generative network prior. This prior is then integrated following a MAP setting, where the data fidelity and prior terms are combined with a fusion weight that is adaptive to both. The BIGPrior framework is a generalization of a large family of classical restoration methods where the prior as well as its contribution weight are both learned, and the weight can adapt to both the signal quality *and* the fitness of the prior to the observed data.

Our framework structurally provides a reliable metric for per-pixel data fidelity in the final output to answer the question of ‘‘How much hallucination is there, at worst, in the output?’’. We present and analyze this metric using blind denoising experiments. We also apply our method to various image restoration tasks and show consistent improvements, notably over the direct use of the generative prior, while providing our faithfulness, or data fidelity, metric.

II. RELATED WORK

A. Classical image restoration

A variety of classical restoration methods such as non-local means (NLM) [4], BM3D [9], their variants [10], [26] or combinations with sparse coding [13], [29], and diffusion-based methods [32], [6], make use of various prior assumptions on self-similarity or frequency-content distribution. Other algorithms formulate the prior explicitly. For instance, dictionary-based methods [35] that assume images can be well represented by a fixed set of elements, which we discuss in the next section. Other examples are shrinkage methods [14], [44]. They can be directly connected with the family of MAP estimators, deriving from the foundational work of Bayes and Laplace [25]. Considering an example with a hyper-Laplacian prior on image gradients, originally used in the context of deblurring in [24], optimizing the MAP negative log-likelihood

$$\arg \min_x -\log(p_{Y|X}(y|x)p_X(x)), \quad (2)$$

yields the estimator

$$\hat{x} = \arg \min_x \|x - y\|_2^2 + \beta \cdot \sum_{j=1}^J |x \otimes f_j|^\gamma, \quad (3)$$

where y is the signal we observe, \hat{x} is the estimate of the target x , $\{f_j\}$ are J first-order derivative filters and β is a weight parameter. Setting γ to one, with the corresponding

filters, gives the special case of total-variation methods [36]. Generally these approaches are an optimization of the form

$$\hat{x} = \arg \min_x \psi_d(x, y) + \beta \cdot \psi_p(\mathcal{T}(x)), \quad (4)$$

where ψ_d is the data-fidelity loss term, and ψ_p incorporates the prior information on a transformation \mathcal{T} of x , which could be the identity. \mathcal{T} can also be based on derivatives [24], or wavelet [37] and other sparsifying transformations. For instance, WNNM [19] assumes that subsets of similar image patches are low-rank and uses a weighted nuclear norm for the low-rank minimization problem on similar patch groups. As with many classical image denoising methods, WNNM adapts β based on the noise level and controls the data fidelity weight as such. However, as we noted in our introduction, these methods face two shortcomings. First, β is not adapted based on the confidence in the prior given the degraded observation, only on the quality of the latter. It is thus adapted based on the signal quality, such as the noise level for instance, but also only following certain heuristics. And second, the prior itself is fixed based on hand-designed heuristics. We aim to preserve an interpretable control over the contribution of the prior and decouple it from data fidelity, while leveraging learned network priors and increasing the flexibility in the fusion weight. This weight is thus *learned* in our framework, and can adapt both to the quality of the observed data as well as the fitness of the prior, given the test observation.

B. Deep neural networks

The rich priors that convolutional neural networks are able to learn have improved image restoration results [20], [49], [50], [48]. These methods leverage sample-based learning and can extract prior information from large image datasets. This has allowed these deep learning methods to improve the state of the art on many restoration tasks [52]. However, the learned priors are implicit, meaning neither the prior nor its contribution can be disentangled from the data fidelity component in the final restored output. As recently shown for super-resolution and denoising tasks [16], networks can learn a frequency-conditional hallucination that is prone to overfitting to the training degradation models. Another recent example is in 3D reconstruction [41], where networks learn to recognize observations and leverage memorized data samples rather than performing the reconstruction. In other words, the prior contribution can dominate over the data fidelity. Controlling this trade-off is, however, not attainable within the neural networks. Our proposed framework allows us to leverage the strength of learned network priors while keeping both control and insight over the data fidelity and prior trade-offs.

Extracting prior information from neural networks is possible through an inversion process [12], [1]. By searching the network-learned space of image distributions, it is possible to project on it in a similar fashion as with dictionary-based methods. Generative networks are sufficiently powerful to be trained to learn different distributions such as image or noise distributions [5]. A network inversion is carried out in [18], where it is used for different image processing tasks. We

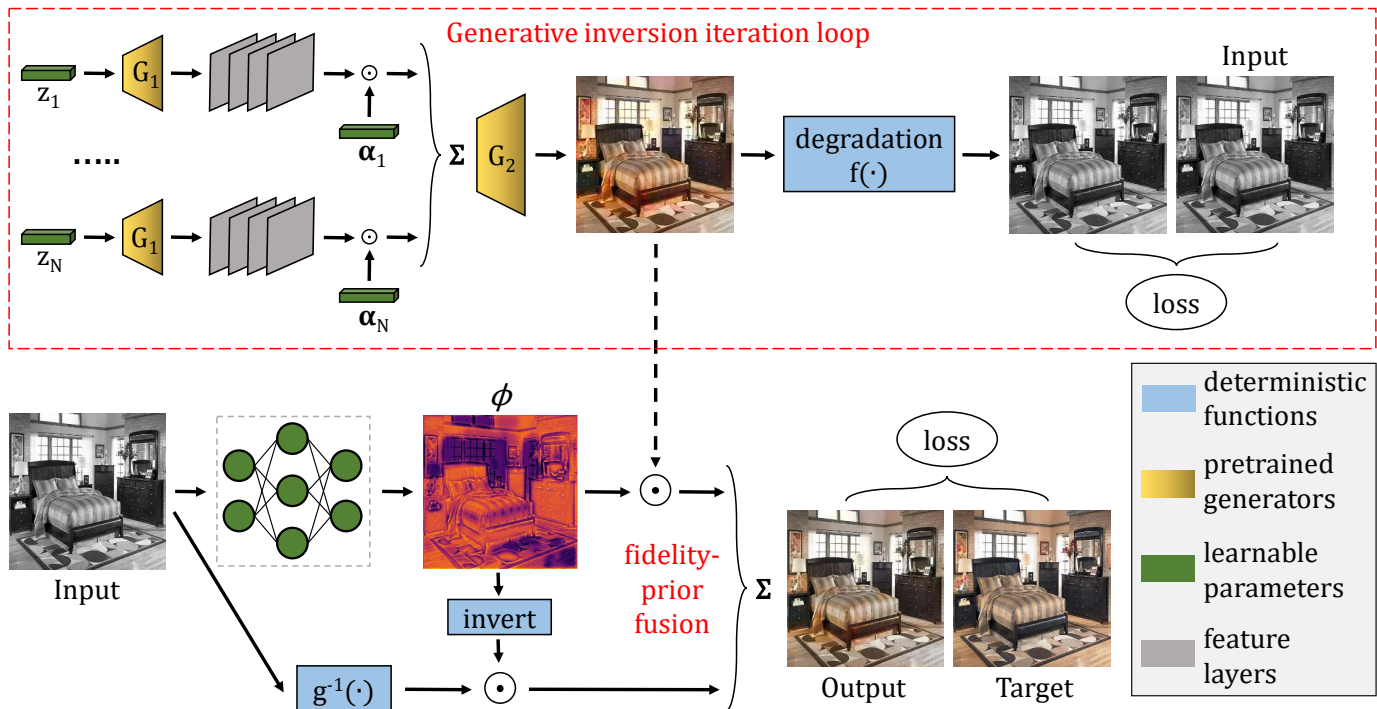


Fig. 1. Weights that are optimized are shown in green, and the sub-networks of the pre-trained generative network are shown in yellow. The generative network inversion process is optimized over a fixed set of iterations, which regularizes the output [42]. The final output is obtained through the fusion of the prior-based hallucination and the signal information, based on our ϕ map estimation.

discuss this in more detail in the following section. A generative network inversion is also conducted in [31]. However, the method performs a fine-tuning of the pre-trained generator that goes against our objective to project on a fixed learned space. We also emphasize that our goal is not to improve such priors, but rather to leverage them in our framework as image-projection spaces.

C. Signal adaptation of priors

As described in our discussion on classical methods, some of them [19] adapt the weight assigned to their prior term according to the quality of the observed signal. However, the fitness of the chosen prior can itself be image dependent. In other words, the prior may be accurate on certain images, but not as fit to be applied to others. Yet this is rarely accounted for in the literature. In the content-aware image prior presented in [7], although the weight of the prior itself is not adaptive, the hyper-Laplacian prior used is tweaked to adjust to the texture in the observed signal. Similarly, the method in [8] carefully selects its filters upon processing of the observed signal, hence altering its implicit priors. Also in the same spirit, some recent deep learning methods try to adapt to the observed inputs, through self-supervised weight modification [27], or novel learning [3], and this approach is even appearing in recent classification work to adjust to distribution shifts [40]. Such methods thus address the issue of the fitness of the prior to the given input by modifying the former on the fly. However, once a prior is selected, its fitness relative to the observed signal’s quality is dismissed. The weight of the prior term is

therefore not adaptive, and the prior’s contribution also cannot be decoupled from data fidelity.

III. METHOD

A. Mathematical formulation

Given an observed signal y that is a degraded version of the image x , our restoration estimate \hat{x} is formulated as

$$\hat{x} = \underbrace{(1 - \phi(y; \theta_1)) \odot g^{-1}(y)}_{\text{data fidelity}} + \underbrace{\phi(y; \theta_1) \odot G(z^*; \theta_2)}_{\text{prior}}, \quad (5)$$

where $g^{-1}(\cdot)$ is a bijective function that we discuss in what follows, $\phi(\cdot; \theta_1)$ is an estimator for the fusion factor, parameterized by θ_1 , that assigns adaptive weights to the prior-based hallucination and the data fidelity. It is a generalization of β that we learn internally from sample-based training. $G(z^*; \theta_2)$ is the prior-based hallucination, parameterized by θ_2 , described in detail in what follows, and \odot is the pixel-wise multiplication operator. To ensure a very strict lossless data fidelity term, we restrict $g^{-1}(\cdot)$ to the set of bijective functions. We can choose it such that $g(\cdot)$ is close to the degradation model $f(\cdot)$ of the restoration task, as described in our experimental setup. We note that this formulation is closely related to the classical restoration methods based on explicit prior optimizations discussed in our related work. The difference is that our prior is based on a trainable neural network G , and that our fusion factor is also learned, to be adaptive per sample both to the quality of the observed data and to the fitness of the prior.

We present the **relation to MAP estimation** in connection with the work in [15]. The authors derive a MAP estimate for Additive White Gaussian Noise (AWGN) removal where the additive noise ($y_i = x_i + n_i$) follows the normal distribution $\mathcal{N}(0, \sigma_n)$, and an explicit image prior is enforced. More precisely, the solution is derived with the assumption of a Gaussian prior [34] *on the pixel distribution*. With this model, the prior distribution for a pixel value x_i follows $\mathcal{N}(\bar{x}_i, \sigma_{x_i})$, and this yields a MAP estimate

$$\hat{x}_i = \arg \max_{x_i} p_{X_i|Y_i}(x_i|y_i) = \frac{y_i}{1 + 1/S_i} + \frac{\bar{x}_i}{1 + S_i}, \quad (6)$$

with S_i being the signal-to-noise ratio defined as

$$S_i \triangleq \frac{\sigma_{x_i}^2}{\sigma_n^2}. \quad (7)$$

Note how S_i is in fact dependent on signal quality (through σ_n) as well as the confidence in the prior (through σ_{x_i}). Indeed, intuitively the larger σ_{x_i} is, the less reliable is the prior term \bar{x}_i , and the smaller it is, the more reliable is the prior term. In this special case of our general formulation,

$$\phi(y_i) = \frac{1}{1 + S_i}, \quad (8)$$

$g(\cdot)$ is the identity mapping, and the prior is the expected value over the distribution of the input $\mathbb{E}_{X_i}[x_i]$. Our formulation in Eq. (5) generalizes this solution to non-Gaussian as well as image-wise prior distributions, while taking into account signal quality and prior confidence.

We also describe the **relation to dictionary-based** methods. Dictionary-based methods [17], [35] generally follow the formulation

$$\hat{x} = \arg \min_{x, d(x, M\omega) < \epsilon} \psi_d(x, y) + \beta \cdot \psi_p(\omega), \quad (9)$$

where M is the dictionary, namely, a vector set spanning the dictionary space, ω holds the coordinates of a point in that space, $d(\cdot, \cdot)$ is a distance function and ϵ is a small value in \mathbb{R}_+ . It is typical to use a ψ_p that encourages sparsity, thus assuming that the dictionary captures the main directions of variation in an image. This sparsity of ω parallels restrictions on the generative latent space. Effectively, enforcing

$$d(x, M\omega) < \epsilon \quad (10)$$

is a subtle relaxation of the constraint $x \in \text{span}(M)$, which enforces the prior assumption that the image must belong to the dictionary space. This would correspond in our formulation of Eq. (5) to $x \in \text{span}(G)$, where in our case the dictionary space is instead the learned space of a generative network. In our formulation, the restriction is only enforced on our decoupled prior element, rather than having to enforce it on x itself and then relaxing it through a tweaking of ϵ .

In summary, our formulation can be viewed as a general framework of MAP estimation, as well as a generalization of dictionary-based methods. We choose a strict data fidelity term preserving a bijective relation to the observed signal, and a fusion factor that takes into account both signal quality and prior confidence. The following two sections discuss in more detail the prior term and the ϕ fusion factor learning.

	ϕ explicitly known	ϕ relation to data fidelity
Colorization	✗	Luminance and edge related
Inpainting	✓	Binary mask based
Denoising	✗	Noise-level adaptive

TABLE I

THE ϕ MAP VALUES ARE ONLY EXPLICITLY KNOWN FOR INPAINTING, BUT ARE ALWAYS RELATED TO THE DATA FIDELITY AND PRIOR CONFIDENCE TERMS DISCUSSED IN OUR MATHEMATICAL FORMULATION. IN COLORIZATION THERE EXIST STRONG RELATIONS BETWEEN LUMINANCE AND THE FIDELITY OF THE OBSERVED DATA, IN INPAINTING THIS DIRECTLY MATCHES THE APPLIED MASK, AND IN DENOISING THE NOISE LEVEL DETERMINES THE FIDELITY OF THE OBSERVATION. THE ϕ MAP ALSO, ACROSS ALL TASKS, DEPENDS ON THE CONFIDENCE IN THE PRIOR.

Method	Bedroom set	Church set
	AuC [50] ↑	AuC [50] ↑
Colorful colorization [50]	<u>88.55</u>	89.13
Deep image prior [42]	84.33	83.31
Feature map opt. [3]	85.41	86.10
mGAN prior [18]	88.52	<u>89.69</u>
Ours	89.27	90.64

TABLE II

QUANTITATIVE AUC (%) RESULTS FOR IMAGE COLORIZATION ON THE BEDROOM AND CHURCH TEST SETS. THE HIGHER THE VALUE, THE LOWER IS THE CUMULATIVE COLORIZATION ERROR CURVE. WE HIGHLIGHT WITH BACKGROUND SHADED IN GRAY THE WIDELY USED TASK-SPECIFIC SUPERVISED METHOD. THE BEST RESULTS ARE SHOWN IN BOLD, AND THE SECOND BEST ARE UNDERLINED.

B. Generative-space projection prior

Theoretically, an inference method can be used to replace the prior term. For instance, a feed-forward network’s output can replace $G(z^*)$ in Eq. (5). However, such a network trained with supervision takes into account both the data fidelity and prior terms, albeit without any insight as to how much prior-based hallucination takes place or any control over the different contributions. Therefore, in order to best decouple data fidelity from prior hallucination, we opt for a pre-trained generative network inversion to act as the learned prior. Effectively, this is a better strategy to decrease the upper bound on a worst-case hallucination contribution. The inversion produces a sampling from the generative space, or a projection on that space as in dictionary-based projections discussed earlier. The latent code z^* for the generative-space projection is obtained as

$$z^* = \arg \min_z \mathcal{L}_G(f(G(z)), y), \quad (11)$$

where \mathcal{L}_G can be a weighted average of ℓ_1 , ℓ_2 , and perceptual losses, and $f(\cdot)$ is the degradation model of a restoration task. Using a single latent code, very limited information can be encoded, which yields a coarse prior notably for high-resolution images. To avoid this expressiveness loss, we leverage the recent multi-code GAN inversion method that splits the generative network G into two stages, at layer l [18]. The first stage $G_1^{(l)}$ generates multiple feature space representations, each corresponding to one of N latent codes $\{z_n^*\}_{n=1}^N$, where every α is a vector of length equal to the number of feature-space channels. The second stage $G_2^{(l)}$ generates the output image based on a fused feature representation



Fig. 2. From left to right are the ground-truth image (GT), the grayscale input, the results of colorful image colorization (CIC) [50], mGAN [18], and ours, with the AuC (%), and our channel-averaged ϕ map (with global average between parentheses). The darker colors indicate values of ϕ closer to 0, while bright yellow indicates those closer to 1.

using adaptive channel weights $\{\alpha_n^*\}_{n=1}^N$. The latent codes and adaptive weights are obtained as in Eq. (11) by an inversion optimization

$$\{z_n^*\}_{n=1}^N, \{\alpha_n^*\}_{n=1}^N = \arg \min_{\{z_n\}_{n=1}^N, \{\alpha_n\}_{n=1}^N} \mathcal{L}(f(x^{inv}), x), \quad (12)$$

where the inverted image x^{inv} is given by

$$G(z; \alpha, \theta_2) \triangleq x^{inv} = G_2^{(l)} \left(\sum_{n=1}^N G_1^{(l)}(z_n) \cdot \alpha_n \right). \quad (13)$$

Our prior term in Eq. (11) is then given by $G(z^*; \alpha^*, \theta_2)$, where θ_2 are the frozen weights of the generative sub-networks G_1 and G_2 . We lastly note that randomly traversing the latent space of a generative network can potentially produce hallucinated images lying outside the natural image manifold [30]. This is fended off by the guided inversion loss that maps the generative output, through the degradation model, to the observed image. The case of the generative projection being outside the natural image manifold, which can occur when the degradation is extreme, still does not pose an issue in our framework. Indeed, this projection is already treated in our approach as a prior hallucination that may or may not be faithful to the original image.

C. Guide-free ϕ learning

A guided learning of the parameters θ_1 to predict ϕ is possible for a task such as inpainting but impossible for other tasks. This is simply because inpainting is the extreme case where signal quality is binary, namely zero at the masked areas. For other tasks, a target ϕ cannot be readily obtained. We thus train a network with weights θ_1 to predict ϕ in an end-to-end manner, with ϕ effectively being an intermediate feature space having no explicit learning loss. Our mini-batch training loss $\mathcal{L}(x, y; \theta_1)$ for learning θ_1 is given by (we use ϕ to also denote the network outputting it, for better readability)

$$\mathcal{L}(x, y; \theta_1, \theta_2) = \|(1 - \phi(y, \theta_1)) \odot g^{-1}(y) + \phi(y, \theta_1) \odot G(z^*; \alpha^*, \theta_2) - x\|_2^2 + \rho \cdot \|\phi(y, \theta_1)\|_1, \quad (14)$$

Method	PSNR \uparrow	SSIM \uparrow	LPIPS \downarrow
DeepFill v2 [47], [48]	26.56	0.9555	0.0191
Feature map opt. [3]	14.75	0.4563	-
Deep image prior [42]	17.92	0.4327	-
mGAN prior [18]	20.55	0.5823	0.2070
Ours	<u>25.32</u>	<u>0.9240</u>	<u>0.0376</u>

TABLE III

QUANTITATIVE PSNR (dB), SSIM, AND LPIPS RESULTS FOR CENTRAL IMAGE INPAINTING. WE MASK OUT A 64×64 PATCH FROM THE CENTER OF EACH INPUT IMAGE. THE TASK-SPECIFIC STATE-OF-THE-ART METHOD IS HIGHLIGHTED WITH BACKGROUND SHADED IN GRAY. THE BEST RESULTS ARE SHOWN IN BOLD, AND THE SECOND BEST ARE UNDERLINED.

Test	Method	PSNR \uparrow	SSIM \uparrow	LPIPS \downarrow
Bed.	mGAN prior [18]	20.34	0.5902	0.2134
	Ours	23.22	0.8598	0.0775
Chu.	mGAN prior [18]	19.33	0.5359	0.2235
	Ours	21.94	0.8509	0.0855
Conf.	mGAN prior [18]	19.38	0.5641	0.2062
	Ours	22.20	0.8318	0.0785

TABLE IV

QUANTITATIVE PSNR (dB), SSIM, AND LPIPS RESULTS FOR RANDOMIZED-MASKING INPAINTING ON THE BEDROOM, CHURCH (OUTDOOR), AND CONFERENCE TEST SETS. THE RANDOMIZED MASKING INCREASES THE DIFFICULTY OF PREDICTING OUR ϕ MAPS. WE COMPARE THE PRIOR-BASED RESULTS TO OURS, TO ANALYZE THE EFFECT OF MASK RANDOMIZATION ON THE PERFORMANCE OUR ϕ PREDICTION COMPARED TO THE CENTRAL INPAINTING TASK.

where ρ is a scalar weight that we discuss next, and the parameters θ_2 of the generative network are the frozen weights of a *pre-trained* generative network. This end-to-end training allows the network predicting ϕ to learn to assess, based on the observation y , the quality of that observed image as well as the fitness of the prior to this observation.

Fidelity-bias balance. For certain image test cases, the quality of the data fidelity term can be very similar to that of the learned prior, at least over some subsets of pixels. This would induce no change in the loss term for varying values of our fusion factor ϕ , as all would result in similar



Fig. 3. From left to right are the ground-truth image (GT), the masked input, the results of DeepFill v2 [47], [48], mGAN [18], and ours, with the PSNR in dB , and our channel-averaged ϕ map (with global average between parentheses). The first two rows show example images from the standard central-inpainting benchmark, and the third row is an example from our randomized-inpainting experiment.

final outputs. However, for these cases, it is not necessary to *hallucinate* information since the data fidelity is also just as accurate. Therefore, we address these edge cases by adding an auxiliary loss on the ℓ_1 norm of ϕ in Eq. (14). This term enforces that the training favors smaller values of ϕ such that the overall contribution of the data fidelity term is maximized when this is not detrimental to the quality of the final output. This fidelity-bias term is weighted by the scalar ρ in Eq. (14).

IV. EXPERIMENTS

We conduct experiments on image colorization, inpainting, and blind AWGN removal. Colorization does not induce an explicit solution for ϕ , aside for certain exceptions we discuss in the next section, such as edges and extreme luminance areas. On the other hand, inpainting induces an explicitly-known solution for ϕ . Lastly, AWGN does not have an explicit solution for ϕ , since the image prior is not explicitly formulated. However, the AWGN experimental setup allows us to analyze the guide-free learning of ϕ which would intuitively fluctuate mainly with the noise level (direct relation), but also marginally with the uncertainty in the prior (opposite relation), as described in Section V. This is summarized in Table I and discussed in the following sections.

A. Experimental setup

As described in Sec. III, we leverage the multi-code GAN inversion approach for our generative-space projection prior.

The pre-trained GAN models, corresponding to each dataset used, are all different versions of the PGGAN [21] network. They are pre-trained on the Bedroom, Church (Outdoor), and Conference room datasets taken from the LSUN database [46]. The details for each experiment follow the settings given by the authors of [18] and are given in the following sections. We note that any generative network, such as DCGAN [33], LR-GAN [45], CVAE-GAN [2], StyleGAN [22], StyleGAN2 [23], or even any future method allowing projections or sampling from a learned image distribution, can be used for the projection prior of our method. To enable direct comparisons with with mGAN [18], we use the PGGAN in our experiments. We use AuC [11], [50], PSNR, SSIM [43], and the perceptual metric LPIPS [51] in our quantitative evaluations.

For our fusion factor learning, we train the same backbone network with the same settings for all of our experiments. The architecture is inspired by [49], and is a residual learning made up of a sequence of convolutional, batch normalization, and ReLU blocks. We omit further architecture details which can be found in our code. We use a batch size of 8, a starting learning rate of 0.01, and a fidelity-bias balancing weight $\rho = 1e - 5$. We train for 25 epochs with random shuffling, and update the learning rate following a cosine annealing with warm restarts scheduler [28]. The restart period is adaptive to the batch size such that it is always 4 epochs. We also note for reproducibility that training with images that are normalized to $[0, 1]$ and then zero-centered is empirically observed to improve the final results. The same normalization is then

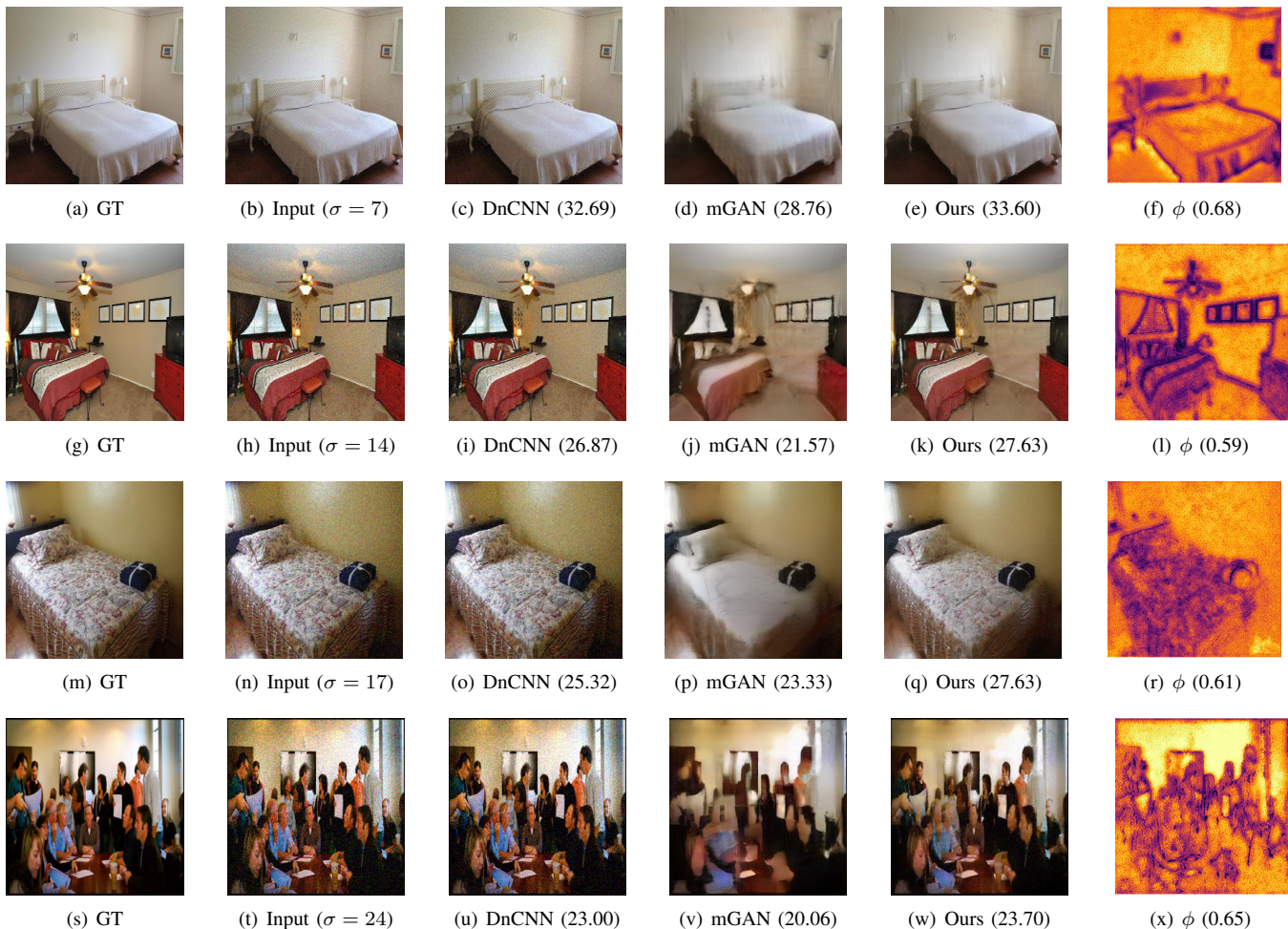


Fig. 4. From left to right are the ground-truth image (GT), the noisy input with the AWGN standard deviation, the results of DnCNN [49], mGAN [18], and ours, with the PSNR in dB , and our channel-averaged ϕ map (with global average between parentheses).

Test	Method	PSNR \uparrow	SSIM \uparrow	LPIPS \downarrow
Bed.	DnCNN [†] [49]	24.96	0.5804	0.1859
	mGAN prior [18]	22.72	0.6257	0.1978
	Ours	26.80	0.7279	0.0998
Church	DnCNN [†] [49]	22.40	0.5166	0.2046
	mGAN prior [18]	21.12	0.5643	0.2065
	Ours	23.38	0.5959	0.1435
Conf.	DnCNN [†] [49]	22.81	0.5310	0.2167
	mGAN prior [18]	21.49	0.5962	0.1968
	Ours	24.70	0.6578	0.1192

TABLE V

PSNR (dB), SSIM, AND LPIPS RESULTS FOR AWGN REMOVAL ON THE BEDROOM, CHURCH, AND CONFERENCE SETS. THE NOISE FOLLOWS A GAUSSIAN DISTRIBUTION WITH STANDARD DEVIATION SAMPLED UNIFORMLY AT RANDOM FROM $[5,50]$ PER IMAGE. [†]WE RETRAIN AND TEST DnCNN WITH THE SAME DATA AND SETUP AS OURS.

performed before inference, and inverted once the output is obtained. We train our model with the loss of Eq. (14) on a subset of the LSUN validation set corresponding to each of the large training sets used for pre-training the PGGAN models, and test on the remaining subset.

B. Colorization

For the colorization of a grayscale input image, unlike inpainting for example, it is much less predictable what an ideal ϕ map would be. We conduct colorization experiments, where the grayscale input is the luminance channel, and we evaluate the error on the ab color space. The AuC metric [11], [50] computes the area under the cumulative percentage ℓ_2 error distribution curve in the ab space. The percentage is that of pixels lying within an error threshold that is swept over $[0, 150]$ in steps of one. For generative network inversion, we use the sixth layer of the PGGAN for the feature composition, with 20 latent codes, and ℓ_2 and VGG-16 perceptual loss [38], optimized with gradient descent for 1500 iterations, following [18]. Our $g^{-1}(y)$ function duplicates the grayscale channel over each of the color channels. The remaining details follow the experimental setup of Sec. IV-A

We present our quantitative image colorization results in Table II, along with those of the deep image prior [42], the feature map optimization [3], the colorful image colorization [50] which is a feed-forward method supervised specifically for colorization, and the mGAN prior [18]. We note the considerable improvement of our method, despite the



Fig. 5. Failure cases of AWGN removal. The quality of the generative network inversion, which remains a very challenging task, is detrimental to our final results. Although our results significantly improve on the prior by leveraging the input observation using our fusion weight, they still fall short of the task-specific DnCNN denoiser’s results.

restriction of enforcing a strict data fidelity.

Visual results are shown in Fig. 2 for the different image colorization methods. We can observe that ϕ is lower on image edges, which indeed generally constitute information that is not lost by the grayscale degradation. We observe as well that ϕ tends to be low when the luminance is around extreme values, since in such cases the grayscale images are faithful to the original color images. In both of these cases, it is the confidence in the data fidelity that gets adapted to the observation. We also note, for instance in the sample of the second row, that ϕ can be very insightful. It indicates that the color of the sky was heavily hallucinated, while the bottom half and the church dome use practically no prior hallucination. This is advantageous for downstream tasks as the dome was, in fact, incorrectly hallucinated by the generative-network projection prior. Similarly for the grass where green was incorrectly added.

Visual results are shown in Fig. 3 for the different methods. For our method, there is little flexibility in terms of the fusion factor ϕ for the inpainting tasks, which are tasks with binary degradation, i.e., the signal is either perfectly available or not

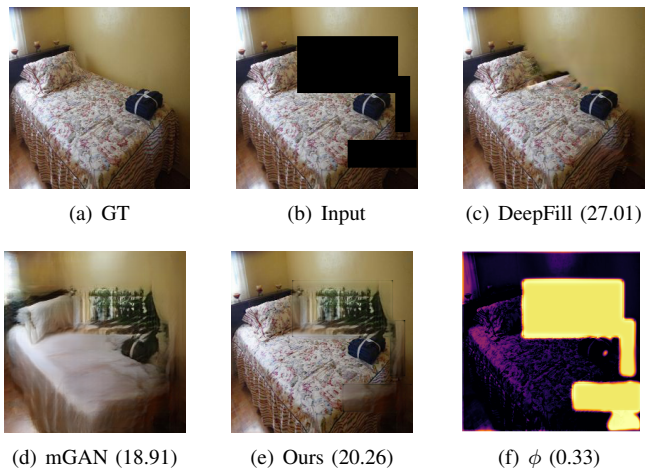


Fig. 6. Failure case in a randomized inpainting experiment. We note a misprediction in the ϕ mask in (f), in the bottom right corner. Our network mistakenly assumed the very dark region to be a masked region. Note that in inpainting, data fidelity cannot be made use of in the masked area, and our results become directly dependent on the quality of the prior, which, in this example, is not high.

at all. The ϕ map effectively predicts the inpainting mask, a mask that is taken as input in the DeepFill method, and our results’ quality is mostly tied to those of the generative network inversion as can be observed visually.

C. Inpainting

We present results on the standard central crop inpainting task in Table III. A 64×64 patch is masked from the test image, and the task is to recover the hidden crop. For generative network inversion, we use the fourth layer of the PGGAN for the feature composition, with 30 latent codes, and ℓ_2 and VGG-16 perceptual loss [38], optimized with gradient descent for 3000 iterations, following [18]. We use an identity function $g^{-1}(y) = y$ for the data fidelity, and the remaining setup follows that of Sec. IV-A. The PSNR, SSIM and LPIPS results show a significant improvement of our approach, due to leveraging the data fidelity, over the mGAN prior results (+4.77dB in terms of PSNR). The inpainting results are averaged across the Bedroom, Church (Outdoor), and Conference datasets. We compare with the deep image prior method [42] and with the recent feature map optimization approach [3] which is a method using GAN priors with test-image specific adaptation. For reference, we compare with a task-specific supervised inpainting method, namely, the most recent version [48] of DeepFill [47], trained on the Places2 dataset. DeepFill takes the mask as input and uses gated convolutions to account for invalid pixel locations, and contextual attention [47] to leverage similar patches across the image. The output is refined by using an adversarial GAN loss on every neuron in the feature space [48]. For inpainting, our approach cannot leverage anything out of the signal over the masked area and is thus dependent on the prior hallucination.

The aforementioned benchmarking setup, however, makes the task simpler for our method in terms of predicting ϕ . Therefore, we design a randomized-masking inpainting setup

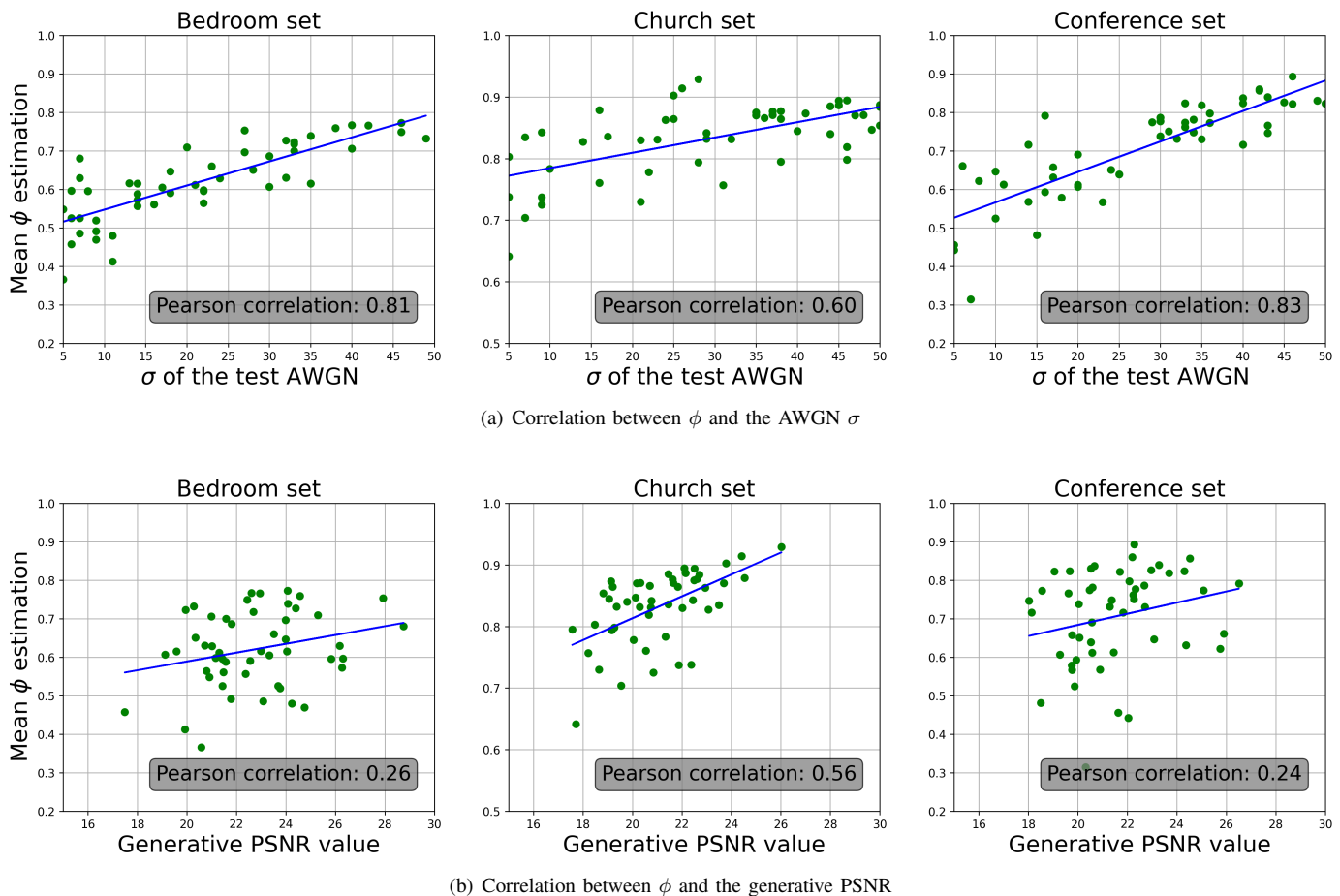


Fig. 7. (a) Shows across three datasets the relation between the AWGN standard deviation in test images, which is directly related to signal quality, and our corresponding mean estimations for ϕ . (b) Shows the same analysis but with respect to the PSNR of the generative network inversion results, which is directly related to the fitness of the prior. Results show a strong Pearson correlation factor between ϕ and signal quality (a), with the remaining factor of variation explained by the fitness of the prior (b) (e.g. Church set).

and present experimental results on it in Table IV. Our randomized-masking algorithm selects uniformly at random a number of patches to be masked, in [2, 4]. Then, per patch, a random pixel location for the corner of that patch is selected. The algorithm lastly samples from a normal distribution $\mathcal{N}(64, 32)$, truncated to [9, $+\infty$), a width and a height for each patch, with re-sampling in case the patch extends beyond the image coordinates. We compare the mGAN prior results with ours in Table IV. We omit the other methods because the goal of this randomized-masking experiment is specifically to analyze the effect of randomizing the mask on our ϕ prediction, and how the incurred errors in ϕ affect the performance relative to the prior. We can first note that the mGAN performance decreases, by almost 0.02 SSIM points on average. With the randomization of the mask, our performance decreases more significantly, by almost 0.1 SSIM points, but still significantly improves over the mGAN results. This comparison highlights the increased difficulty of our internal ϕ prediction when the mask is randomized relative to the central inpainting task where the mask location is immutable.

D. Blind denoising

We conduct experiments on blind denoising, specifically on AWGN removal. For blind denoising, we follow the standard setup [49], [15], [16] of sampling a noise level uniformly at random over the range [5, 50]. This level is the standard deviation of the AWGN. For generative network inversion, we use the fourth layer of the PGGAN for the feature composition, with 30 latent codes, and ℓ_2 and VGG-16 perceptual loss [38], optimized with gradient descent for 3000 iterations, following [18]. We set $f(\cdot)$ (Eq. (11)) to the identity. Our $g^{-1}(y)$ function is also the identity function as the noise is zero-mean. Generally, $g^{-1}(\cdot)$ can be the subtraction of the noise mean value. For the remaining setup details, we follow the experimental setup of Sec. IV-A.

We present the AWGN removal results in Table V, along with those of DnCNN [49], which we retrain on the same data as ours. Our approach achieves the best performance consistently across the different datasets and evaluation metrics.

Visual results are shown in Fig. 4 for the different methods. We observe that DnCNN preserves details well, but at the cost of poorer denoising on low-frequency regions (e.g. walls). The mGAN results are worse than DnCNN, but with our

framework the final results become more visually pleasing and accurate. The ϕ map illustrates per pixel the contribution of hallucination relative to data fidelity, and is again lower around edges, as with colorization. We analyze ϕ in more detail, in the context of AWGN removal, in the next section.

V. DISCUSSION

The AWGN experiments provide the ideal setup for an analysis of ϕ , which we carry out in this section. We know that ϕ should be inversely related to the signal quality, the poorer the signal the higher the ϕ values. And ϕ is then also directly related to the confidence in the prior, or the fitness thereof. With AWGN, the quality of the signal is also inversely related to the noise level, in this case, to the standard deviation of the Gaussian noise. We thus analyze the correlation between the mean ϕ value for a test image, and the standard deviation of the noise in that test image. Results are shown in Fig. 7(a), with the Pearson correlation factor, for three datasets. We can clearly observe the positive correlation between the two variables, with a factor of 0.83 and 0.81 for the bedroom and conference sets, respectively. The correlation is lower, at 0.6, for the church dataset. The remaining factor of variability in ϕ is the fitness of the prior, which we analyze in Fig. 7(b). The correlation between the average ϕ value and the generative PSNR is the highest for the church set, reaching 0.56, and supporting our claims with regard to ϕ . Indeed, we observe that ϕ is well-correlated with the signal’s quality, and when that correlation is somewhat lower it is matched with a higher correlation between ϕ and the fitness of the prior, exactly as expected from the MAP framework’s perspective. To summarize, we make two supporting observations from our aforementioned analysis. First, the ϕ estimation, which is learned with no guide in our framework, strongly correlates with the signal quality. Second, a lower correlation with signal quality, as in the church set, is directly justified by a higher correlation between ϕ and the fitness of the prior to the test data. These two observations exactly align with the intuitions derived from the MAP estimation framework as presented in Section III-A.

The framework we present can be a novel basis for image restoration as it can counter the obstacle of degradation-model overfitting, common in image restoration tasks. This is because hallucination is structurally the key part prone to overfitting to the chosen model. Our framework can guard against that type of overfitting by relying on decoupled data fidelity and prior hallucination, and using a pre-trained and frozen generative network, independent of the degradation model, for the hallucination part. Our fusion factor could also be used to increase the robustness and reliability of downstream computer vision tasks, by making the latter aware of the extent of per-pixel hallucination in the restoration result. For instance, when a computer vision algorithm deals with degraded images, rather than training the downstream network only on the restoration output, further information regarding the degree of hallucination can be leveraged to increase robustness, notably against adversarial attacks. Our fusion map ϕ conveys such hallucination information, which

can also be used for better interpretability of the results by human users.

VI. CONCLUSION

We present a framework for image restoration that enables the use of deep networks for extracting an image prior while decoupling prior-based hallucination and data fidelity. We show how our framework is a generalization of a large family of classical restoration methods, notably of a Bayesian MAP estimation setup, and of dictionary-based restoration methods.

We conduct experiments on image colorization, inpainting, and Gaussian denoising. Our results, which structurally come with a pixel-wise map indicating data fidelity versus prior hallucination contributions, outperform prior-based methods and are even competitive with state-of-the-art task-specific supervised methods. We lastly present an analysis of this fusion factor ϕ estimation that supports our different claims.

REFERENCES

- [1] Michael Albright and Scott McCloskey. Source generator attribution via inversion. In *CVPR Workshops*, 2019. 2
- [2] Jianmin Bao, Dong Chen, Fang Wen, Houqiang Li, and Gang Hua. CVAE-GAN: fine-grained image generation through asymmetric training. In *ICCV*, pages 2745–2754, 2017. 6
- [3] David Bau, Hendrik Strobelt, William Peebles, Bolei Zhou, Jun-Yan Zhu, Antonio Torralba, et al. Semantic photo manipulation with a generative image prior. *arXiv preprint arXiv:2005.07727*, 2020. 3, 4, 5, 7, 8
- [4] Antoni Buades, Bartomeu Coll, and J-M Morel. A non-local algorithm for image denoising. In *CVPR*, pages 60–65, 2005. 1, 2
- [5] Jingwen Chen, Jiawei Chen, Hongyang Chao, and Ming Yang. Image blind denoising with generative adversarial network based noise modeling. In *CVPR*, pages 3155–3164, 2018. 2
- [6] Yunjin Chen, Wei Yu, and Thomas Pock. On learning optimized reaction diffusion processes for effective image restoration. In *CVPR*, pages 5261–5269, 2015. 2
- [7] Taeg Sang Cho, Neel Joshi, C Lawrence Zitnick, Sing Bing Kang, Richard Szeliski, and William T Freeman. A content-aware image prior. In *CVPR*, pages 169–176, 2010. 3
- [8] Sungjoon Choi, John Isidoro, Pascal Getreuer, and Peyman Milanfar. Fast, trainable, multiscale denoising. In *ICIP*, pages 963–967, 2018. 3
- [9] Kostadin Dabov, Alessandro Foi, Vladimir Katkovnik, and Karen Egiazarian. Image denoising by sparse 3-D transform-domain collaborative filtering. *IEEE TIP*, 16(8):2080–2095, 2007. 1, 2
- [10] Kostadin Dabov, Alessandro Foi, Vladimir Katkovnik, and Karen Egiazarian. BM3D image denoising with shape-adaptive principal component analysis. In *Signal Processing with Adaptive Sparse Structured Representations*, 2009. 2
- [11] Aditya Deshpande, Jason Rock, and David Forsyth. Learning large-scale automatic image colorization. In *ICCV*, pages 567–575, 2015. 6, 7
- [12] Jeff Donahue, Philipp Krähenbühl, and Trevor Darrell. Adversarial feature learning. In *ICLR*, 2017. 2
- [13] Weisheng Dong, Guangming Shi, Xin Li, Yi Ma, and Feng Huang. Compressive sensing via nonlocal low-rank regularization. *IEEE TIP*, 23(8):3618–3632, 2014. 2
- [14] David L Donoho. De-noising by soft-thresholding. *IEEE Transactions on Information Theory*, 41(3):613–627, 1995. 2
- [15] Majed El Helou and Sabine Süsstrunk. Blind universal Bayesian image denoising with Gaussian noise level learning. *IEEE TIP*, 29:4885–4897, 2020. 1, 4, 9
- [16] Majed El Helou, Ruofan Zhou, and Sabine Süsstrunk. Stochastic frequency masking to improve super-resolution and denoising networks. In *ECCV*, 2020. 2, 9
- [17] Raja Giryes and Michael Elad. Sparsity-based Poisson denoising with dictionary learning. *IEEE TIP*, 23(12):5057–5069, 2014. 4
- [18] Jinjin Gu, Yujun Shen, and Bolei Zhou. Image processing using multi-code GAN prior. In *CVPR*, pages 3012–3021, 2020. 2, 4, 5, 6, 7, 8, 9
- [19] Shuhang Gu, Lei Zhang, Wangmeng Zuo, and Xiangchu Feng. Weighted nuclear norm minimization with application to image denoising. In *CVPR*, pages 2862–2869, 2014. 2, 3

- [20] Viren Jain and Sebastian Seung. Natural image denoising with convolutional networks. In *NeurIPS*, pages 769–776, 2009. [2](#)
- [21] Tero Karras, Timo Aila, Samuli Laine, and Jaakko Lehtinen. Progressive growing of GANs for improved quality, stability, and variation. In *ICLR*, 2018. [1](#), [6](#)
- [22] Tero Karras, Samuli Laine, and Timo Aila. A style-based generator architecture for generative adversarial networks. In *CVPR*, pages 4401–4410, 2019. [1](#), [6](#)
- [23] Tero Karras, Samuli Laine, Miika Aittala, Janne Hellsten, Jaakko Lehtinen, and Timo Aila. Analyzing and improving the image quality of StyleGAN. In *CVPR*, pages 8110–8119, 2020. [1](#), [6](#)
- [24] Dilip Krishnan and Rob Fergus. Fast image deconvolution using hyper-Laplacian priors. In *NeurIPS*, pages 1033–1041, 2009. [1](#), [2](#)
- [25] Pierre-Simon Laplace. *Pierre-Simon Laplace Philosophical Essay on Probabilities: Translated from the fifth French edition of 1825 With Notes by the Translator*, volume 13. Springer Science & Business Media, 1998. [2](#)
- [26] Marc Lebrun, Antoni Buades, and Jean-Michel Morel. A nonlocal Bayesian image denoising algorithm. *SIAM Journal on Imaging Sciences*, 6(3):1665–1688, 2013. [2](#)
- [27] Seunghwan Lee, Donghyeon Cho, Jiwon Kim, and Tae Hyun Kim. Self-supervised fast adaptation for denoising via meta-learning. *arXiv preprint arXiv:2001.02899*, 2020. [3](#)
- [28] Ilya Loshchilov and Frank Hutter. SGDR: Stochastic gradient descent with warm restarts. In *ICLR*, 2017. [6](#)
- [29] Julien Mairal, Francis Bach, Jean Ponce, Guillermo Sapiro, and Andrew Zisserman. Non-local sparse models for image restoration. In *ICCV*, pages 2272–2279, 2009. [2](#)
- [30] Sachit Menon, Alexandru Damian, Shijia Hu, Nikhil Ravi, and Cynthia Rudin. PULSE: Self-supervised photo upsampling via latent space exploration of generative models. In *CVPR*, pages 2437–2445, 2020. [5](#)
- [31] Xingang Pan, Xiaohang Zhan, Bo Dai, Dahua Lin, Chen Change Loy, and Ping Luo. Exploiting deep generative prior for versatile image restoration and manipulation. In *ECCV*, 2020. [3](#)
- [32] Pietro Perona and Jitendra Malik. Scale-space and edge detection using anisotropic diffusion. *IEEE TPAMI*, 12(7):629–639, 1990. [1](#), [2](#)
- [33] Alec Radford, Luke Metz, and Soumith Chintala. Unsupervised representation learning with deep convolutional generative adversarial networks. *arXiv preprint arXiv:1511.06434*, 2015. [6](#)
- [34] Sami Romdhani and Thomas Vetter. Estimating 3D shape and texture using pixel intensity, edges, specular highlights, texture constraints and a prior. In *CVPR*, pages 986–993, 2005. [4](#)
- [35] Ron Rubinstein, Tomer Peleg, and Michael Elad. Analysis K-SVD: A dictionary-learning algorithm for the analysis sparse model. *IEEE TSP*, 61(3):661–677, 2012. [2](#), [4](#)
- [36] Leonid I Rudin, Stanley Osher, and Emad Fatemi. Nonlinear total variation based noise removal algorithms. *Physica D: nonlinear phenomena*, 60(1-4):259–268, 1992. [2](#)
- [37] Sylvain Sardy, Paul Tseng, and Andrew Bruce. Robust wavelet denoising. *IEEE TSP*, 49(6):1146–1152, 2001. [2](#)
- [38] Karen Simonyan and Andrew Zisserman. Very deep convolutional networks for large-scale image recognition. In *ICLR*, 2015. [7](#), [8](#), [9](#)
- [39] Vishwanath A Sindagi, Poojan Oza, Rajeev Yasarla, and Vishal M Patel. Prior-based domain adaptive object detection for hazy and rainy conditions. In *ECCV*, 2020. [1](#)
- [40] Yu Sun, Xiaolong Wang, Zhuang Liu, John Miller, Alexei A Efros, and Moritz Hardt. Test-time training with self-supervision for generalization under distribution shifts. In *ICML*, 2020. [3](#)
- [41] Maxim Tatarchenko, Stephan R Richter, René Ranftl, Zhuwen Li, Vladlen Koltun, and Thomas Brox. What do single-view 3D reconstruction networks learn? In *CVPR*, pages 3405–3414, 2019. [2](#)
- [42] Dmitry Ulyanov, Andrea Vedaldi, and Victor Lempitsky. Deep image prior. In *CVPR*, pages 9446–9454, 2018. [3](#), [4](#), [5](#), [7](#), [8](#)
- [43] Zhou Wang, Alan C Bovik, Hamid R Sheikh, and Eero P Simoncelli. Image quality assessment: from error visibility to structural similarity. *IEEE TIP*, 13(4):600–612, 2004. [6](#)
- [44] Jinjun Xu and Stanley Osher. Iterative regularization and nonlinear inverse scale space applied to wavelet-based denoising. *IEEE TIP*, 16(2):534–544, 2007. [2](#)
- [45] Jianwei Yang, Anitha Kannan, Dhruv Batra, and Devi Parikh. LR-GAN: Layered recursive generative adversarial networks for image generation. In *ICLR*, 2017. [6](#)
- [46] Fisher Yu, Ari Seff, Yinda Zhang, Shuran Song, Thomas Funkhouser, and Jianxiang Xiao. LSUN: Construction of a large-scale image dataset using deep learning with humans in the loop. *arXiv preprint arXiv:1506.03365*, 2015. [6](#)
- [47] Jiahui Yu, Zhe Lin, Jimei Yang, Xiaohui Shen, Xin Lu, and Thomas S Huang. Generative image inpainting with contextual attention. In *CVPR*, pages 5505–5514, 2018. [5](#), [6](#), [8](#)
- [48] Jiahui Yu, Zhe Lin, Jimei Yang, Xiaohui Shen, Xin Lu, and Thomas S Huang. Free-form image inpainting with gated convolution. In *ICCV*, pages 4471–4480, 2019. [2](#), [5](#), [6](#), [8](#)
- [49] Kai Zhang, Wangmeng Zuo, Yunjin Chen, Deyu Meng, and Lei Zhang. Beyond a Gaussian denoiser: Residual learning of deep CNN for image denoising. *IEEE TIP*, 26(7):3142–3155, 2017. [2](#), [6](#), [7](#), [9](#)
- [50] Richard Zhang, Phillip Isola, and Alexei Efros. Colorful image colorization. In *ECCV*, pages 649–666, 2016. [2](#), [4](#), [5](#), [6](#), [7](#)
- [51] Richard Zhang, Phillip Isola, Alexei Efros, Eli Shechtman, and Oliver Wang. The unreasonable effectiveness of deep features as a perceptual metric. In *CVPR*, pages 586–595, 2018. [6](#)
- [52] Yulun Zhang, Kunpeng Li, Kai Li, Bineng Zhong, and Yun Fu. Residual non-local attention networks for image restoration. In *ICLR*, 2019. [2](#)